View metadata, citation and similar papers at core.ac.uk

brought to you by CORE

provided by CURVE/open

Automotive catalyst design for uniform conversion efficiency

Benjamin, S.F. , Liu, Z. and Roberts, C.A.

Author post-print (accepted) deposited in CURVE June 2013

Original citation & hyperlink:
Benjamin, S.F. , Liu, Z. and Roberts, C.A. (2004) Automotive catalyst design for uniform conversion efficiency. Applied Mathematical Modelling, volume 28 (6): 559–572
http://dx.doi.org/10.1016/j.apm.2003.10.008

Copyright © and Moral Rights are retained by the author(s) and/ or other copyright owners. A copy can be downloaded for personal non-commercial research or study, without prior permission or charge. This item cannot be reproduced or quoted extensively from without first obtaining permission in writing from the copyright holder(s). The content must not be changed in any way or sold commercially in any format or medium without the formal permission of the copyright holders.

This document is the author's post-print version of the journal article, incorporating any revisions agreed during the peer-review process. Some differences between the published version and this version may remain and you are advised to consult the published version if you wish to cite from it.

CURVE is the Institutional Repository for Coventry University
http://curve.coventry.ac.uk/open

Automotive Catalyst Design for Uniform Conversion Efficiency

S. F. Benjamin, Z. Liu and C. A. Roberts

Centre for Automotive Engineering Research and Technology

School of Engineering, Coventry University, Priory St. Coventry CV1 5FB

UK

Abstract

This paper describes a computational fluid dynamics (CFD) technique for the prediction of uniform conversion efficiency across the monolith of an automotive catalytic converter. Upstream packaging constraints invariably lead to maldistributed flow and hence variable conversion efficiency across the monolith. The technique described here gives predictions of cell size and/or monolith length distributions such that the conversion efficiency is spatially uniform across the monolith for the general case of a non-uniform flow distribution. The technique applies to the case of mass transfer limited conversion, which is the predominant mode of operation through vehicle drive cycles.

Keywords: automotive catalyst, CFD, conversion efficiency

NOTATION

A channel cross sectional area

C concentration in the channel

C_o concentration at channel inlet

C_{wall} concentration at the wall

D_m molecular diffusivity

d channel hydraulic diameter

h mass transfer coefficient

k turbulent kinetic energy

K constant

L real channel length

$\bar{L}$ uniform artificial channel length

P channel perimeter

Δp pressure loss

n cell density

Re Reynolds number

Sh Sherwood number, $\frac{dh}{D_m}$

U mean channel velocity

U_s superficial channel velocity

u superficial velocity component

$|\boldsymbol{v}|$ superficial velocity magnitude

x distance along channel

w wall thickness

α, β permeability constants in pressure loss expression

ε turbulent kinetic energy dissipation rate

η conversion efficiency

η_c constant conversion efficiency

Λ constant parameter, $\frac{\ln(1-\eta_c)}{4 \cdot Sh \cdot D_m}$

μ dynamic viscosity

ψ monolith porosity

1 INTRODUCTION

The design of automotive after-treatment systems to meet emission regulations has been the subject of considerable research over several decades [1]. Currently, three-way catalytic converters are widely used to reduce emissions of carbon monoxide (CO), hydrocarbons (HC) and nitrogen oxides (NOx) formed during the combustion process. Automotive catalysts comprise of either ceramic or metallic monolith structures featuring many parallel channels of small hydraulic diameter ~ 1mm. This provides the high surface area required for maximum conversion efficiency. Widely used ceramic monoliths normally comprise of channels of square cross section with cell densities varying between 31-93 cells/cm^2. The monolith is coated with a thin washcoat, within which are embedded the precious metal catalysts, normally platinum or palladium and rhodium. When the catalyst is active HC, CO and NOx, once diffused to the washcoat, are converted through chemical reactions. The overall heterogeneous reaction rate is a function of the rate of mass transfer to the washcoat surface and the chemical reaction rate within the washcoat. Only when the temperature of the monolith has reached about 500K, the light-off temperature, will significant reactions occur. Up to this time the reaction rate is chemically controlled. Post light-off reaction rates are mass transfer limited. Conversion efficiency is then a function of residence time within the monolith, the surface to volume ratio of the monolith and the mass transfer coefficient. For typical vehicle drive cycles the catalyst is predominantly operating in the mass transfer regime.

The design of the converter varies considerably. Early converters were situated underneath the vehicle, a metre or two downstream of the engine. For these

underbody designs the exhaust ports usually discharge into a common downpipe prior to entering the catalyst. The required volume of the monolith depends on many factors, not least the engine capacity. For reduced pressure drop the monolith is normally designed to have as short a length as possible. Typically, cylindrical monoliths will have diameters ~ 100mm and lengths ~ 150mm requiring a large expansion from the exhaust pipe to the front face of the substrate. Unfortunately packaging constraints often do not permit the use of long diffusers. Hence flow separation within the diffuser is commonplace leading to a non-uniform flow distribution across the monolith. It is not unusual for maximum flow velocities within the substrate to be a factor of two greater than the mean [2]. With the introduction of tighter emission legislation the need to reduce light-off times by increasing the rate of catalyst warm-up has also become important. One way to achieve this is to place converters closer to the engine, the so-called close-coupled catalyst (CCC) design. CCC systems typically feature each exhaust port discharging directly into the upstream diffuser. Vehicles often feature a combination of CCC and underbody catalysts. The CCC is used to achieve rapid warm-up with the underbody catalyst reducing emissions post light-off.

For either type of converter maldistributed flow affects catalyst warm-up, light-off time, deactivation, conversion efficiency and system pressure loss. It also results in large sections of the catalyst being poorly utilised [2-9]. Hence considerable effort is directed towards improving the flow distribution within manufacturing/packaging constraints. Whilst much experimental flow work has been undertaken using flow rigs and engine studies [10-15] there has been, over the last decade or two, an increasing use of computational fluid dynamics (CFD) to predict the performance of the

converter. Studies have ranged from isothermal flow investigations [16-18] to simulations in which the flow, heat and mass transfer and chemical kinetics have been modelled [19-20]. The flow in the upstream diffuser and manifolds is obtained through solution of the Reynolds-Averaged Navier-Stokes (RANS) equations. The monolith itself is normally treated as a porous medium with properties (porosity, flow resistance, conductivity, thermal capacity etc) governed by the geometric configuration of the channels within the monolith and its material composition. Once these are prescribed then for given inlet and boundary conditions a CFD solution can readily be obtained. By changing either the geometry of the upstream diffuser and/or monolith dimensions (cell density, length etc.) various designs can be simulated and the most promising manufactured and tested. An interesting approach to the problem has been reported in the work of Comfort [4] and by Kavounis and Assanis. [6]. These authors were primarily concerned with the effect of flow maldistribution on emissions post light-off. The latter used CFD to simulate the flow distribution within a monolith. Once a flow solution was obtained then a simple model of mass transfer limited conversion was applied to predict emissions across the monolith. They investigated the effect of cell density and Re on conversion efficiency. A similar simple approach under pulsating flow conditions has recently been reported by Jeong and Kim [21].

In most studies the monoliths have relatively simple shapes. Most have plane ends normal to the axis of the monolith and uniform cell distributions-these being the simplest designs for manufacturing purposes. Recently there have been a number of studies reported for monoliths with shaped ends and varying cell distributions. Various authors have investigated using contoured monoliths featuring either cone or

dome-shaped ends [22-24]. The idea behind these designs is to force the flow towards the periphery of the monolith to provide a more even flow distribution. Petters et al [25] describe monoliths with both front and rear shaped faces. Kim and Son [26] describe a concept whereby the cell distribution is allowed to vary across the monolith. In their work CFD simulations were performed for monoliths with a higher cell density in the center. The idea here was that the high resistance at the center would help to spread the flow more favourably across the monolith. In another study, Maus et al [27] describe the construction of a metallic monolith that allowed channel density to vary from the front to the rear of the monolith within a contoured face design.

The conventional approach in using CFD to design more efficient catalysts necessarily involves a fair degree of trial and error no matter how well informed the practitioner may be. There does not seem to be a methodology that predicts catalyst geometry directly. This paper outlines such a methodology. It provides a method for achieving uniform conversion efficiency under diffusion-controlled conditions for the general case of a non-uniform flow distribution across the catalyst. Such conditions apply after catalyst light-off, the normal operating state. The criterion of uniform conversion efficiency across the monolith is chosen as this represents the optimum design concept.

2. METHODOLOGY

Consider the conversion efficiency for the case of a catalytic converter operating in the mass transfer limited regime under steady state conditions and a typical monolith channel as shown in figure 1. Under such conditions conversion efficiency can be obtained using the Sherwood number (*Sh*), a fundamental non-dimensional parameter for mass transfer.

Treating the flow as one-dimensional and neglecting axial diffusion then a simple mass balance can be performed on a channel element of length δx by equating the net advection into the element with mass transfer to the channel walls,

$$(UAC)_x - (UAC)_{x+\delta x} = hP\delta x[C(x) - C_{wall}] \quad (1)$$

Hence

$$C(x) = C_o \exp(-\frac{hPx}{UA}) \quad (2)$$

Here it is assumed that the temperatures are sufficiently high for the surface reaction rates to be much faster than the mass transfer rate to the channel walls and hence wall concentrations can be assumed to be negligibly small. Defining a channel hydraulic diameter, $d=4A/P$, then with the mass transfer coefficient h defined as

$$h = \frac{Sh \cdot D_m}{d} \quad (3)$$

the concentration at the channel exit is

$$C(L) = C_o \exp(-\frac{4L \cdot Sh \cdot D_m}{Ud^2}) \quad (4)$$

and we can define a conversion efficiency η as,

$$\eta = \frac{C_o - C(L)}{C_o} = 1 - \exp(-\frac{4L \cdot Sh \cdot D_m}{Ud^2}) \quad (5)$$

Once the flow field is known or assumed then equation 5 gives the conversion efficiency directly. A similar approach can be found in work of Comfort [4], Karvounis and Assanis [6] and Jeong and Kim [21].

Consider a monolith comprised of numerous such channels. It is convenient to define a monolith superficial velocity, U_s that assumes all the porous medium is fluid, i.e. there is negligible wall thickness, *w*. Without loss of generality it is convenient to consider the case for channels of square section, the shape normally associated with ceramic monoliths. For this case for a substrate porosity, ψ and cell density, *n* we have

$$U = \frac{U_s}{\psi} = \frac{U_s}{nd^2} = U_s\left(\frac{d+w}{d}\right)^2 \quad (6)$$

If a uniform conversion efficiency η_c is required across the monolith then according to equation 5 and 6 we must have for all channels

$$\frac{\psi L}{d^2} = \frac{L}{(d+w)^2} = -\left(\frac{\ln(1-\eta_c)}{4 \cdot Sh \cdot D_m}\right) U_s = \Lambda U_s \qquad (7)$$

This suggests that for a given flow distribution there is an infinite number of combinations of monolith parameters that can be chosen to give a uniform conversion efficiency across the monolith. For example if the monolith length and wall thickness are fixed and constant then the channel hydraulic diameter, *d* is given by

$$d = \sqrt{\frac{L}{\Lambda U_s}} - w \qquad (8)$$

Alternatively if the channel hydraulic diameter and wall thickness are fixed and constant (hence monolith porosity is constant), then the monolith length is given by

$$L = \frac{\Lambda U_s d^2}{\psi} = \Lambda U_s (d+w)^2 \qquad (9)$$

In both cases *d* and *L* will vary across the monolith because in general U_s will vary but the conversion efficiency for all channels is constant i.e. optimum use of the monolith is ensured. This assumes of course that the distribution of U_s is known a-priori.

The flow distribution across the monolith is governed by the upstream geometry and monolith resistance, this being a function of U_s and monolith dimensions. Hence an iterative design approach is needed. Such an iterative solution is in principle possible using CFD. As mentioned earlier the monolith normally is treated as a porous

medium. The flow in the monolith is made unidirectional by applying large transverse resistances whereas in the flow direction the pressure loss is normally described by the Hagen-Poisieulle relationship for fully developed laminar flow; the maximum channel *Re* being typically in the range 400-1500. Hence within the channel the pressure loss can be described as,

$$\Delta P = \frac{K\mu UL}{d^2} = \frac{K\mu U_s L}{\psi d^2} = \frac{K\mu (d+w)^2 U_s L}{d^4} \tag{10}$$

where K=28.454 for cells of square cross-sectional area. Equation 10 neglects other losses associated with the developing boundary layer and entrance effects [28]. These can be included but for the sake of simplicity and without loss of generality equation 10 will be considered here.

By way of example if we are given values of η_c, L and w then equations 8 and 10 give

$$\Delta P = \frac{K\mu L^2}{\Lambda\left(\sqrt{\frac{L}{\Lambda U_s}} - w\right)^4} \tag{11}$$

Alternatively for given values of η_c, d and w equations 9 and 10 give

$$\Delta P = \frac{K\mu\Lambda (d+w)^4}{d^4} U_s^{\,2} \tag{12}$$

Utilising equations 11 and 12 for the flow resistance will therefore provide iterative solutions to the velocity distribution U_s across the substrate ensuring uniform conversion is achieved within each channel. For the first case the channel hydraulic diameter d is subsequently obtained from equation 8 and for the latter case the channel length L is obtained by equation 9.

3. CASE STUDIES

To illustrate the technique two isothermal simulations are presented for axi-symmetric systems using the STAR-CD CFD code [29]. The geometry is shown in figure 2 (a) and represents an underbody type of converter. The mesh comprises 10 blocks of cells. A 96mm long inlet pipe (blocks 1, 2, 6 and 7) of diameter 48.5mm leads into a conical diffuser (blocks 3 and 8) of half angle 30 degree. A 152mm long monolith (blocks 4 and 9) of diameter 118mm is located downstream of the diffuser followed by a 30mm long outlet sleeve (blocks 5 and 10). The mesh comprises 78 radial cells (58 for blocks 1-5 and 20 in the near wall region, blocks 6-10) and 363 axial cells. A higher axial density of cells was used in the diffuser and the short inlet section immediately upstream (blocks 2, 3, 7 and 8). In a previous study by Wollin [31], a grid refinement exercise was conducted on the same geometry. Cell densities (radial x axial) were varied from (50x162) to (110x389) cells. A grid of (78x363) cells gave a total pressure loss only 1.7% different from the latter. This density was thus considered sufficiently refined to be used for the present study. Since the whole system is axi-symmetric only a 5-degree wedge was simulated with the two side faces defined as symmetry planes. Other boundaries used are inlet boundary, outlet boundary and non-slip wall. The RANS equations were solved in all blocks except 4

and 9 in which the Hagen-Poisieulle relationship was applied. The equations were solved using the SIMPLE algorithm (semi-implicit method for pressure-linked equations) [29]. The second order differencing scheme MARS [29] was used for momentum variables and the first order upwind differencing scheme for turbulence variables. The quadratic non-linear *k*-ε model [29] was used except near the walls where the Norris & Reynolds one-equation model [29] was applied.

The temperature was fixed at 700K, thus ensuring that conversion efficiency was mass transfer limited and air properties appropriate for this temperature were used. Unless stated otherwise a conversion efficiency η_c of 99% was assumed and the inlet mass flow rate was taken as ~70g/s. This gives an inlet velocity of 75m/s with a corresponding *Re* ~ 55000. The inlet velocity was assumed to be uniform and steady. For the monolith, STAR-CD allows implementation of pressure loss expressions in one of two ways. User specified momentum sinks can be added to a special subroutine or alternatively a general pressure loss expression is provided by STAR-CD of the form

$$\frac{\Delta p}{L} = (\alpha|\boldsymbol{v}| + \beta)u \qquad (13)$$

where u is the superficial velocity in one of the three orthotropic directions, α and β are user-supplied permeability constants in that direction and $|\boldsymbol{v}|$ is the superficial velocity magnitude.

3.1 Case 1-variable hydraulic diameter

For this case substrate resistance was given by equation 11 (L and w fixed, d variable). The expression, due to its complication, was entered as a user specified momentum sink, which is a function of U_s. The channels were assumed square with K=28.454, L =152mm and w=0.1625mm.

Figure 3 shows predictions of the velocity profile at the exit plane through the monolith and the channel hydraulic diameter distribution as deduced from equation 8, which will provide 99% uniform conversion efficiency across the monolith. To check the accuracy of the methodology a simulation was performed to verify the predicted velocity profile in case 1 using the block structure in figure 2a. Again the user subroutine to define the pressure loss as a momentum sink was utilized and the pressure loss expression was given by equation 10. The channel hydraulic diameter d, however, was allowed to vary across the radius of the porous medium as previously predicted (figure 3). Figure 4 shows that the two velocity profiles are almost identical and that the conversion efficiency for the verification case is uniform.

Figure 3 shows that predicted channel hydraulic diameters near the wall are unrealistically high due to the reduced velocities in this region. Clearly it would not be possible to configure such a monolith. For this reason a simplified distribution was investigated as shown in figure 5. For this case all channel hydraulic diameters within 12mm of the periphery were fixed at 1.89mm whilst those in the central region were unchanged. A simulation was performed for this simplified hydraulic diameter distribution. Again equation 10 was used as the pressure loss expression in the user subroutine to define the momentum sink using the simplified channel diameter

distribution. Figure 6 shows conversion efficiencies for the simplified distribution and the verification case. The mass-weighted average conversion efficiency has been only slightly reduced to 98.8%.

3.2 Case 2-variable monolith length

Flow conditions were identical to case 1. The substrate resistance, however, was given by equation 12 (*d* and *w* fixed, *L* variable). This pressure loss was implemented by applying equation 13. The permeability constants were defined such that α and β in the transverse direction were given large values (of order 10^6) whilst in the channel flow direction β was given a very small value (10^{-6}) and α was given by

$$\alpha = \frac{K\mu\Lambda(d+w)^4}{\overline{L}d^4} \tag{14}$$

The hydraulic diameter was chosen as 1.105mm, wall thickness 0.1625mm (equivalent to porosity 76%), *K*=28.454, and $\overline{L}$ =152mm. The block structure shown in figure 2(a) was used for this case. In order to perform the simulation an artificial substrate "length" $\overline{L}$ is required in the model. This is purely a means of prescribing the correct overall resistance as required by equation 12.

Figure 7 shows the predicted velocity profile at the exit plane through the monolith and the channel length distribution as deduced from equation 9. Using the predicted channel length distribution a model with a contoured monolith (porous medium) was set up and the simulation performed to verify the prediction accuracy for case 2. The

monolith geometry was such that the front face of the catalyst was assumed flat whilst the rear was contoured, as shown in figure 2 (b), in which blocks 4 and 9 represent the contoured monolith. Clearly if the front face were to be contoured the flow distribution would be significantly influenced by other factors over and above monolith resistance [22-24]. The number of cells per block was kept the same as that in figure 2 (a). Flow resistance was given by equation 10 with the channel length prescribed according to figure 7. Again the permeability constants α and β defined in the pressure loss equation 13 were given large values (of order 10^6) in the transverse direction whilst in the channel flow direction α was given a very small value (10^{-6}) and β was given by

$$\beta = \frac{K\mu(d+w)^2}{d^4} \tag{15}$$

Figure 8 shows that the two velocity profiles are almost identical. To illustrate the advantage of using the contoured substrate another simulation was made using a monolith with the same volume as the contoured one. A schematic of the block structure for this case ("equal volume") is shown in figure 2 (c) and again the same number of cells per block was used in this mesh. The substrate has a uniform length of 71.9 mm. The predicted superficial velocity profile at the exit plane of the substrate is shown in figure 8. The flow for the "equal volume" case is more maldistributed due to the reduced resistance in the centre of the monolith. Figure 9 shows conversion efficiencies. The verification simulation shows uniform conversion efficiency of 99%. For the "equal volume" case the monolith is clearly poorly utilised as conversion efficiencies are non-uniform. Lower conversion efficiencies are observed near the

axis and the residence times are clearly too long towards the periphery. Overall mass-weighted average conversion efficiency for the “equal volume” case was only 96.2%.

Finally, a simulation similar to case 2 was performed for a conversion efficiency of 95% with an inlet mass flow of 120g/sec. Figure 2(d) shows the contoured substrate design for uniform conversion efficiency and figure 2(e) shows the equivalent “equal volume” substrate. For both cases the number of cells per block was kept the same as in the previous simulations. Fig 10 shows the conversion efficiencies for this case. The mass-weighted conversion efficiency for the “equal volume “ substrate is only 84.8%.

4. CONCLUSIONS

The principle of a design methodology has been described that predicts the monolith geometry of a catalytic converter under diffusion-limited regimes so as to provide a uniform conversion efficiency across the monolith. The method predicts cell size and/or monolith length distributions such that the conversion efficiency is spatially uniform across the monolith for the general case of a non-uniform flow distribution. The simulations were performed for 2D axisymmetric systems under steady flow conditions and assumed a monolith resistance given by the Hagen-Poiseuille relationship. There is no reason why the technique cannot be extended to more complex geometric configurations and/or incorporate other pressure loss expressions.

REFERENCES

1. Heck R. M. and. Farrauto R. J, Catalytic Air Pollution Control, Van Nostrand Reinhold, 1995.

2. Benjamin S. F., Clarkson R. J., Haimad N. et al**.,** An experimental and predictive study of the flow in axisymmetric automotive exhaust catalyst systems, SAE Transactions, Journal of Fuels and Lubricants, 1996, Vol. 105, Section 4, 1008-1019.

3. Howitt, J. S. and Sekella, T.C., Flow Effects in Monolithic Honeycomb Automotive Catalytic Converters, SAE Paper No. 740244, 1974.

4. Comfort E. H**.,** Monolithic catalytic converter performance as a function of flow distribution, ASME Winter Annual Meeting, Paper No. 74-WA/HT-30, 1974

5. Zygourakis K., Transient operation of monolith catalytic converters: a two-dimensional reactor model and the effects of radially nonuniform flow distributions, Chemical Engineering Science, 1989, 44 (9), 2075-2086.

6. Karvounis E. and Assanis D. N**.,** The effect of inlet flow distribution on catalytic conversion efficiency, Int. J. Heat Mass Transfer, 1993, 36 (6), 1495-1504.

7. Kim J.Y., Lai M.-C. , Li P. et al., Flow distribution and pressure drop in diffuser-monolith flows, Transactions of the ASME Sept 1995, 117, 362-368.

8. Martin A. P., Will N. S., Bordet A. et al., Effect of flow distribution on emissions performance of catalytic converters, SAE Paper No. 980936, 1998.

9. Benjamin S. F. and Roberts C.A., Warming automotive catalysts with pulsating flows, Proc. Instn Mech Engns , 2001, 215, Part D, 891-910.

10. Zhao F-Q., Li L., Xie X. and Lai M-C, An experimental study of the flow structure inside the catalytic converter of a gasoline engine, SAE Paper No. 950784, 1995.

11. Bressler H. , Rammoser D. , Neumaier H. et al., Experimental and predictive investigation of a closed coupled catalytic converter with pulsating flow, SAE Paper No. 960564, 1996.

12. Zhao F-Q., Bai L., Liu Y et al., Transient flow characteristics inside the catalytic converter of a firing gasoline engine, SAE Paper No. 971014, 1997.

13. Bai L., Zhao F-Q, Liu Y. et al., Transient flow and pressure characteristics inside a closed-coupled catalytic converter, SAE Paper No. 982548, 1998.

14. Cho Y-S., Kim D-S., Han M. H. et al., Flow distribution in a close-coupled catalytic converter, SAE Paper No. 982552, 1998.

15. Benjamin S. F., Roberts C. A. and Wollin J**.,** A study of pulsating flow in automotive catalyst systems, Experiments in Fluids, 2002, 33, 629-639.

16. Lai M.-C., Kim J. Y., Cheng C.-Y. et al., Three-dimensional simulations of automotive catalytic converter internal flow, SAE Paper No. 910200, 1991.

17. Weltens H., Bressler H., Terres F. et al., Optimisation of catalytic converter gas flow distribution by CFD, SAE Paper No. 930780, 1993.

18. Jeong S.J. and Kim T. H., CFD investigation of the 3-Dimensional Unsteady Flow in the Catalytic Converter, SAE Paper No 971025, 1997.

19. Clarkson R.J., Benjamin S.F., Jasper T. S. et al**.,** An integrated computational model for the optimisation of monolith catalytic converters, Proceedings IMechE/SAE VTMS Conference, Columbus, Ohio, SAE P-263 Paper No. SAE931071, 1993, 11-24.

20. Jeong Soo-Jin and Kim Woo-Seung, A numerical approach to investigate transient thermal and conversion characteristics of automotive catalytic converter, SAE Paper No 980881, 1998.

21. Jeong S-J and Kim W-S, A three-dimensional numerical study of the effect of pulsating flow on conversion efficiency inside a catalytic converter, Proc Inst Mech Engns , 2001, 215, Part D, 45-61.

22. Wollin J. and Benjamin S. F., A study of the flow performance of ceramic contoured substrates for automotive exhaust catalyst systems, SAE Transactions, Journal of Fuels and Lubricants, 1999, Vol. 108, Section 4, 2014-2021.

23. Heibel A. and Spaid M. A. A., A new converter concept providing improved flow distribution and space utilization, SAE Spring Fuels and Lubricants, SAE Paper No.990768, 1999

24. Holmgren A., Gronstedt T. and Anderson B., Improved flow distribution in automotive monolithic converters, React. Kinet. Catal. Lett., Vol 1997, 60, No2, 363-371.

25. Pelters S., Kaiser F. W. and Mauss W., The development and application of a metal supported catalyst for Porsche's 911 Carrera 4, SAE Paper No 890488, 1989.

26. Kim J. Y. and Son S., Improving Flow Efficiency of a Catalytic Converter Using the Concept of Radially Variable Cell Density-Part I, SAE Paper No 1999-01-0769, Advanced Converter Technologies (SP-1409), 1999.

27. Maus W and Bruck R., The Conical Catalytic Converter and its Potential for Future Close-Coupled Converter Concepts, SAE Paper No 980414, 1998.

28. Benjamin S. F., Haimad N., Roberts C. A. et al., Modelling the flow distribution through automotive catalytic converters, Proc Instn Mech Engrs., 2001, 255, Part C, 379-383.

29. Computational Dynamics, STAR-CD Users Guide and Methodology-Version 3.100B, 1999.

30. Wollin J., A study of pulsating flow in automotive exhaust catalyst systems, PhD thesis, Coventry University, 2002.

Figure 1 Monolith channel

Figure 2 Computational domain and block structure. (a) (70g/sec, η_c =99%), (b) contoured monolith (70g/sec, η_c =99%), (c) “equal volume” monolith, (70g/sec), (d) contoured monolith (120g/sec, η_c =95%), (e) equal volume monolith (120g/sec).

Figure 3 Predicted velocity profile and channel hydraulic diameter distribution for uniform conversion efficiency across the monolith for case 1 (70g/sec, η_c =99%).

Figure 4 Velocity profiles and conversion efficiency for verification
case 1 (70g/sec, η_c =99%).

Figure 5 Simplified distribution of channel hydraulic diameter for
case 1 (70g/sec, η_c =99%).

Figure 6 Comparison of conversion efficiency for the verification case and simplified channel hydraulic diameter distribution for case 1 (70g/sec, η_c =99%).

Figure 7 Predicted velocity profiles and monolith lengths for uniform conversion efficiency across the monolith for case 2 (70g/sec, η_c =99%).

Figure 8 Comparison of the predicted, verification and "equal volume" velocity profiles for case 2 (70g/sec, η_c =99%).

Figure 9 Comparison of conversion efficiencies for the verification and "equal volume" simulations for case 2 (70g/sec, η_c =99%).

Figure 10 Comparison of conversion efficiencies for the verification and "equal volume" simulations for case 2 (120g/sec, η_c =95%).

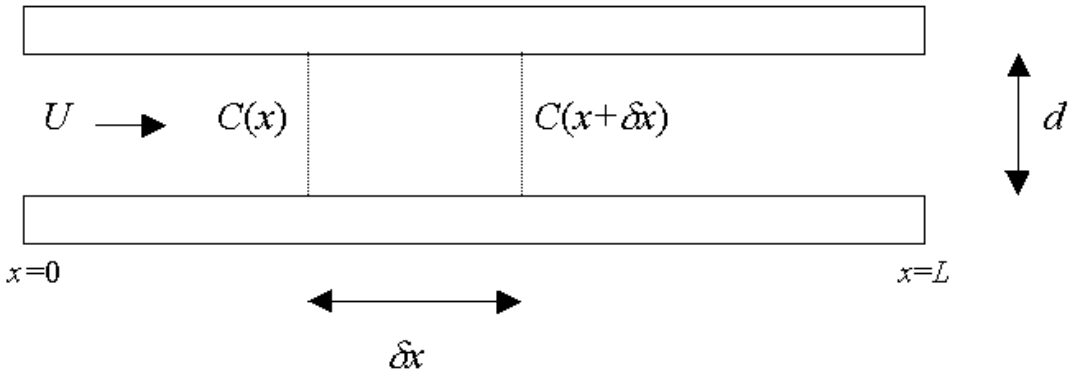

Figure 1

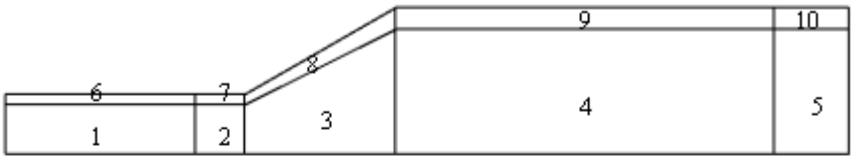

figure 2(a)

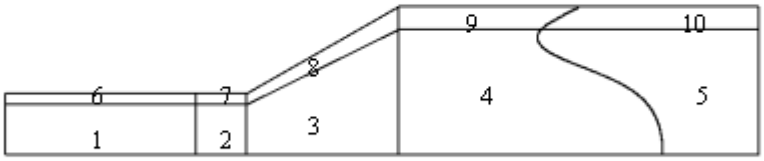

figure 2(b)

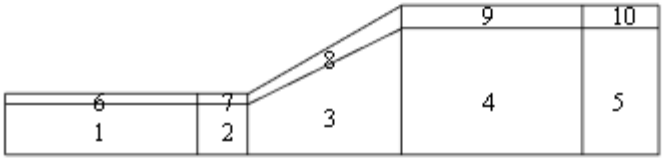

figure 2(c)

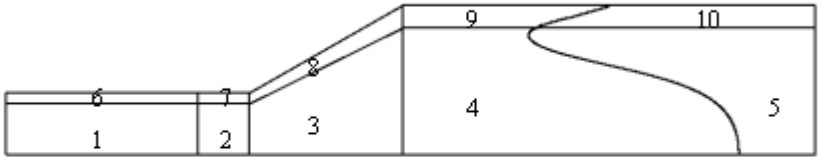

figure 2(d)

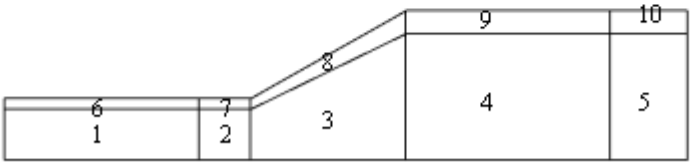

figure 2(e)

Figure 2

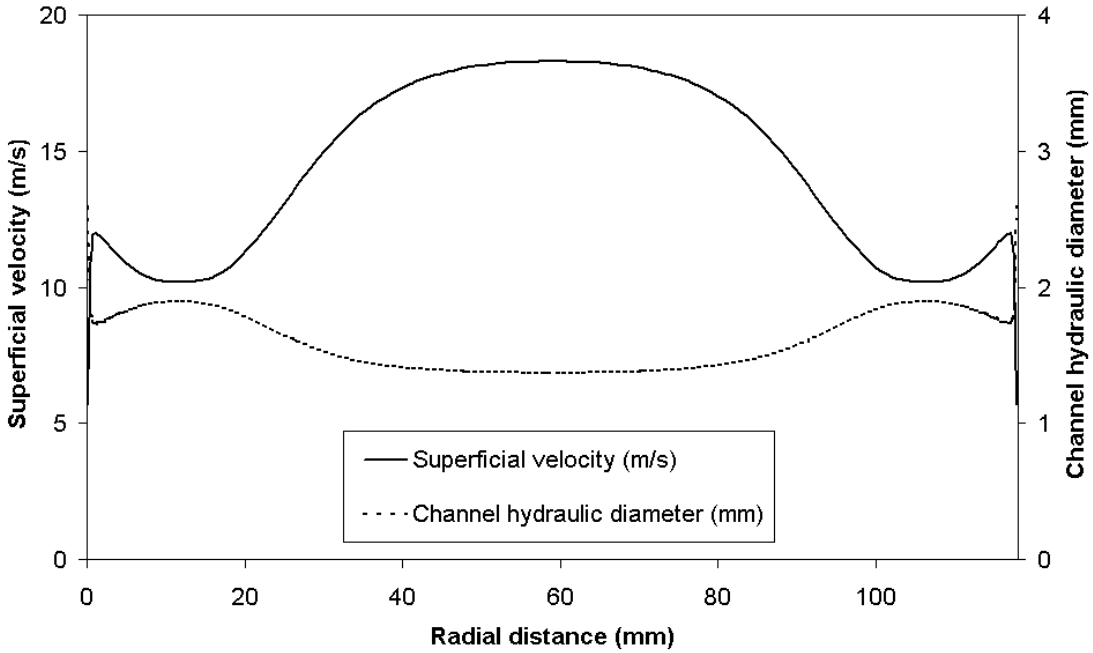
Superficial velocity (m/s)
Channel hydraulic diameter (mm)
Radial distance (mm)
Superficial velocity (m/s)
Channel hydraulic diameter (mm)
0
5
10
15
20
0
1
2
3
4
0
20
40
60
80
100

Figure 3

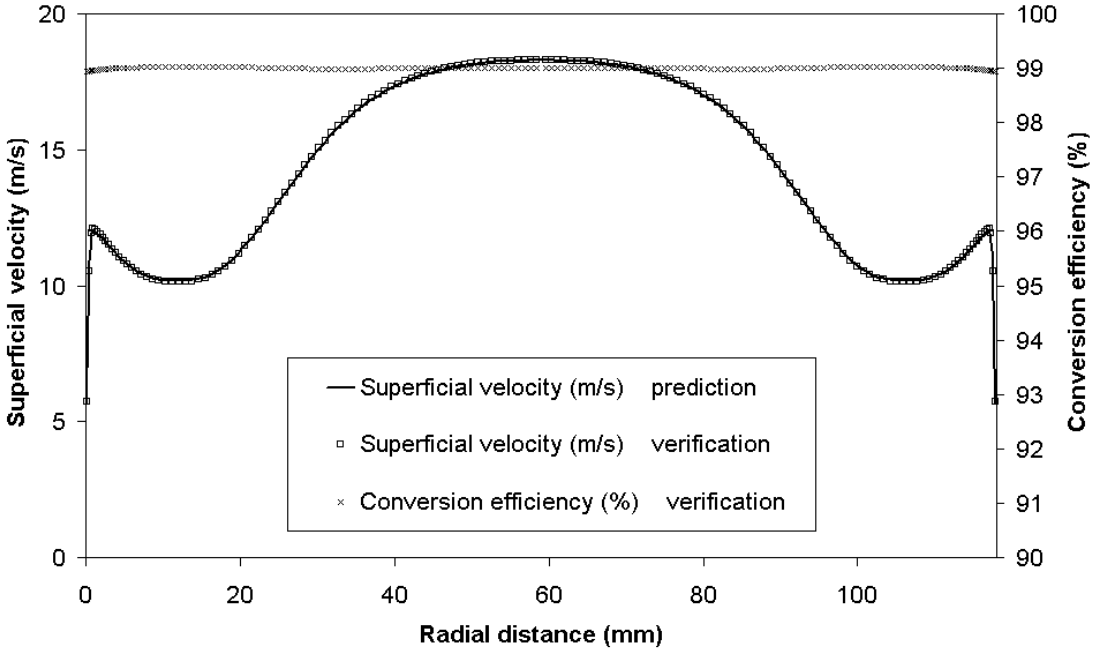
Superficial velocity (m/s)
Conversion efficiency (%)
Radial distance (mm)
Superficial velocity (m/s) prediction
Superficial velocity (m/s) verification
Conversion efficiency (%) verification
0
5
10
15
20
90
91
92
93
94
95
96
97
98
99
100
0
20
40
60
80
100

Figure 4

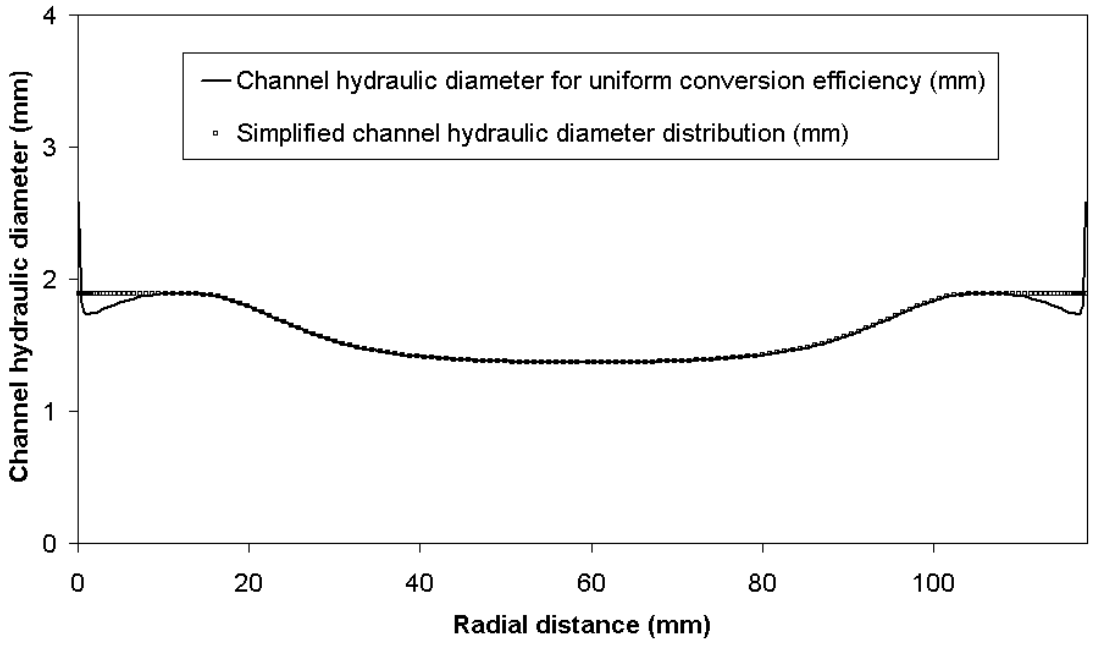
Channel hydraulic diameter for uniform conversion efficiency (mm)
Simplified channel hydraulic diameter distribution (mm)
Channel hydraulic diameter (mm)
Radial distance (mm)
0
1
2
3
4
0
20
40
60
80
100

Figure 5

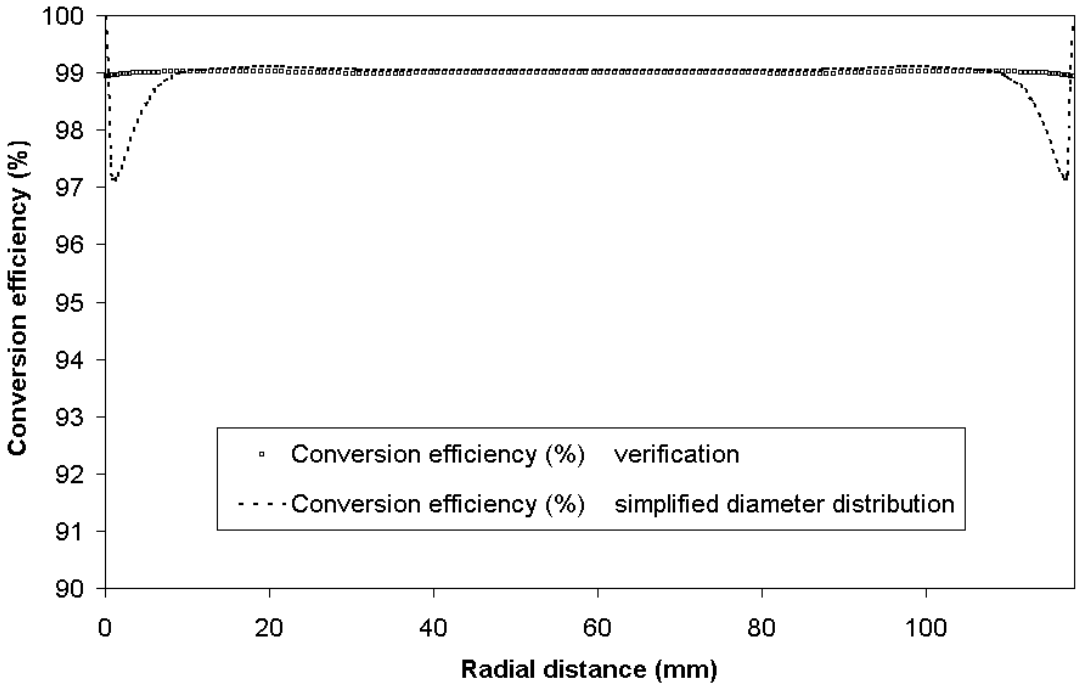
Conversion efficiency (%)
100
99
98
97
96
95
94
93
92
91
90
0
20
40
60
80
100
Radial distance (mm)
Conversion efficiency (%) verification
Conversion efficiency (%) simplified diameter distribution

Figure 6

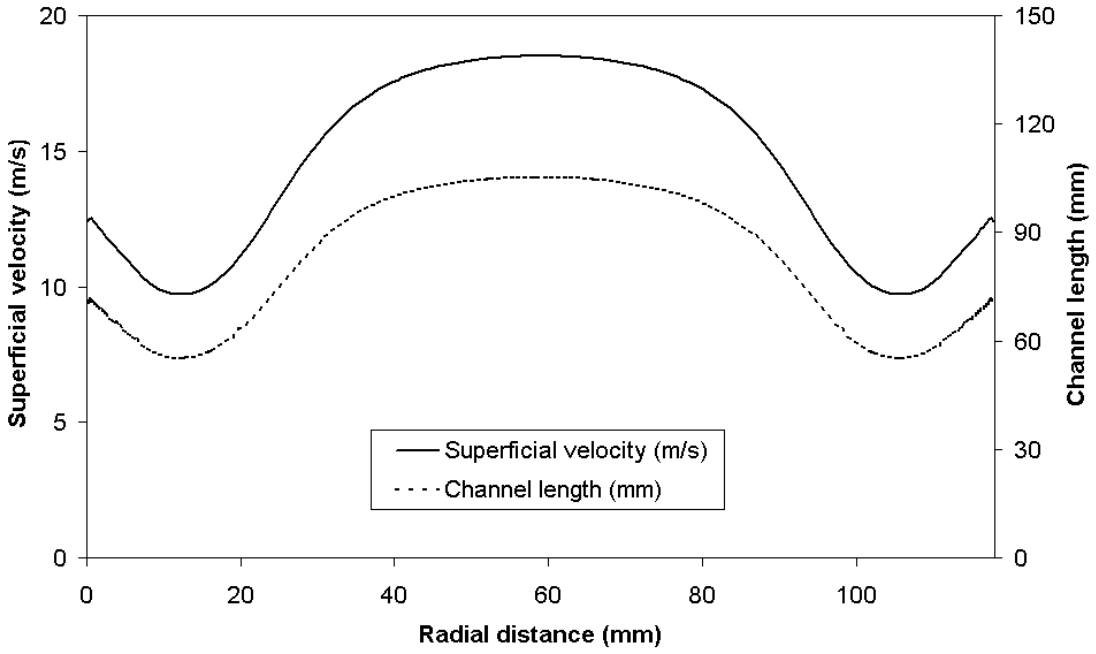
Superficial velocity (m/s)
Channel length (mm)
Radial distance (mm)
Superficial velocity (m/s)
Channel length (mm)
0
5
10
15
20
0
30
60
90
120
150
0
20
40
60
80
100

Figure 7

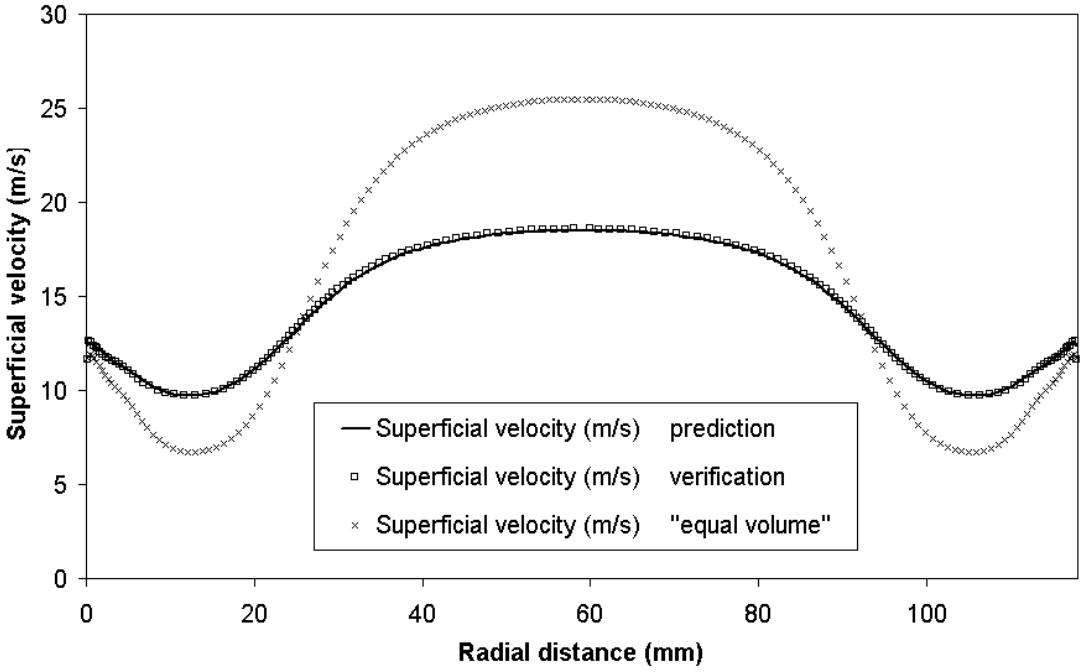
Superficial velocity (m/s)
Radial distance (mm)
0
5
10
15
20
25
30
0
20
40
60
80
100
Superficial velocity (m/s) prediction
Superficial velocity (m/s) verification
Superficial velocity (m/s) "equal volume"

Figure 8

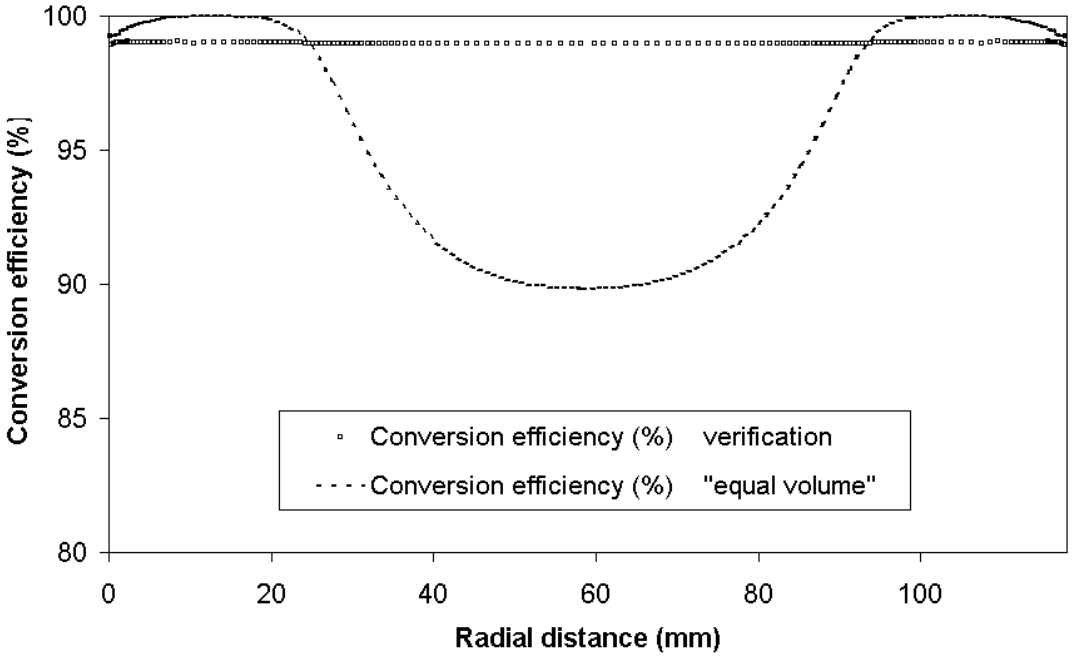
100
95
90
85
80
Conversion efficiency (%)
0
20
40
60
80
100
Radial distance (mm)
Conversion efficiency (%) verification
Conversion efficiency (%) "equal volume"

Figure 9

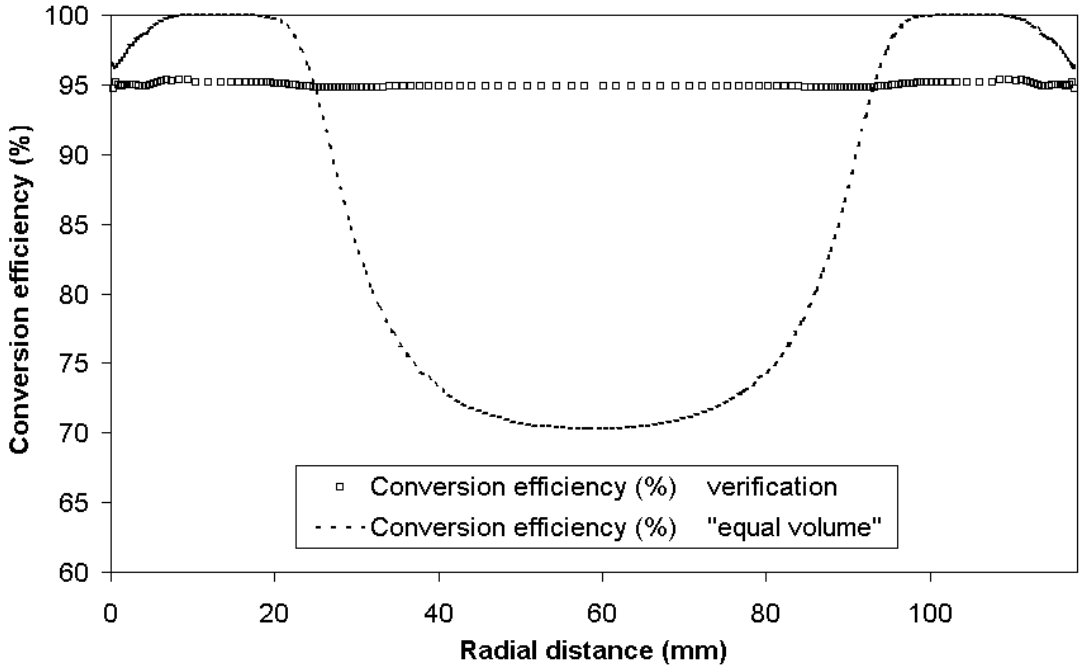
Conversion efficiency (%)
100
95
90
85
80
75
70
65
60
0
20
40
60
80
100
Radial distance (mm)
Conversion efficiency (%) verification
Conversion efficiency (%) "equal volume"

Figure 10